System Response to Gas Production from a Heterogeneous Hydrate Accumulation at the UBGH2-6 Site of the Ulleung Basin in the Korean East Sea

George J. Moridis[1,2], Matthew T. Reagan[1,*], Alejandro F. Queiruga[1],
and Se-Joon Kim[3]

[1]Energy Geosciences Division, Lawrence Berkeley National Laboratory, Berkeley, CA 94720, USA
[2]Department of Petroleum Engineering, Texas A&M University, College Station, TX 77843, USA
[3]Petroleum and Marine Division, Korea Institute of Geoscience and Mineral Resources, Daejeon, Korea

Corresponding author: Matthew T. Reagan (mtreagan@lbl.gov)

Abstract

We investigate the feasibility of production from a layered marine gas hydrate reservoir using the properties and conditions corresponding to the UBGH2-6 site of the Ulleung Basin in the Korean East Sea. The work expands and furthers previous investigations in support of a proposed field test. The target system is location in deep water and consists of 13 m of alternating hydrate-bearing sand and soft mud layers and will be produced using a vertical well. We assess production potential during a 14-day field test, examine sensitivity to heterogeneity in permeability, porosity, and initial hydrate saturation, and assess the geomechanical response of the system to short-term production. Producing gas from the system appears to be technically feasible, however, low production rates and relatively large water production rates are expected during the field test. Expected subsidence and reservoir compaction is limited given the current data and the short timeframes of the production test.

Keywords: Ulleung Basin, Gas Hydrates, Reservoir Simulation, Geomechanical Simulation

1. Introduction

This study is a continuation and expansion of earlier studies by Lawrence Berkeley National Laboratory (LBNL) and the Korea Institute

of Geoscience and Mineral Resources (KIGAM) in support of a planned short-term field test (Moridis et al., 2009; 2013). We use the most recent flow and geomechanical properties of the sediments at the UBGH2-6 site, as gleaned from core analyses and advanced geophysical surveys. The objective of this study is to quantify by means of numerical simulation the response of the hydrate accumulation at the UBGH2-6 site during a short-term field test (14-day long) and determine the feasibility of gas production through depressurization-induced dissociation. In contrast to the earlier studies that assumed homogeneous hydrate-bearing formations and mud interlayers, the current study considers a heterogeneous system, which requires a complex, three-dimensional simulation. The study assesses gas production performance of the accumulation and estimates the sensitivity of production on the parameters that earlier studies identified as having the most pronounced effects on the system behavior and response. In addition, when CH_4 is produced from the hydrate reservoirs, flow is tightly coupled to mechanics because the changes of P and T strongly affect the effective stresses acting on the porous media of the reservoir (Kim et al., 2012a;b; Rutqvist and Moridis, 2009; Rutqvist et al. 2009). Thus, we also investigate the geomechanical response of the reservoir during production, and the connection between production and geomechanical response.

2. System Description and Production Strategy

The discussion and analysis in this section hews very closely to an earlier study (Moridis et al., 2013). Although the basic geological model and the production strategy remain the same as in the earlier study, new data, the consideration of heterogeneity, and the use of a 3D domain results in a drastically different reservoir simulation, with different grid geometry and different porous media properties.

2.1. System description and geometry

This study focuses on the oceanic hydrate deposits located in the Ulleung basin, continuing the previous studies of Moridis et al. (2013). The basin is located in the Korean East Sea, between the Korean Peninsula and Japan. A map of the region is shown in Figure 1. The depth of the seafloor is between 1,500m and 2,300m, and the depth at the site in question, the UBGH2-6 site, is 2,157m.

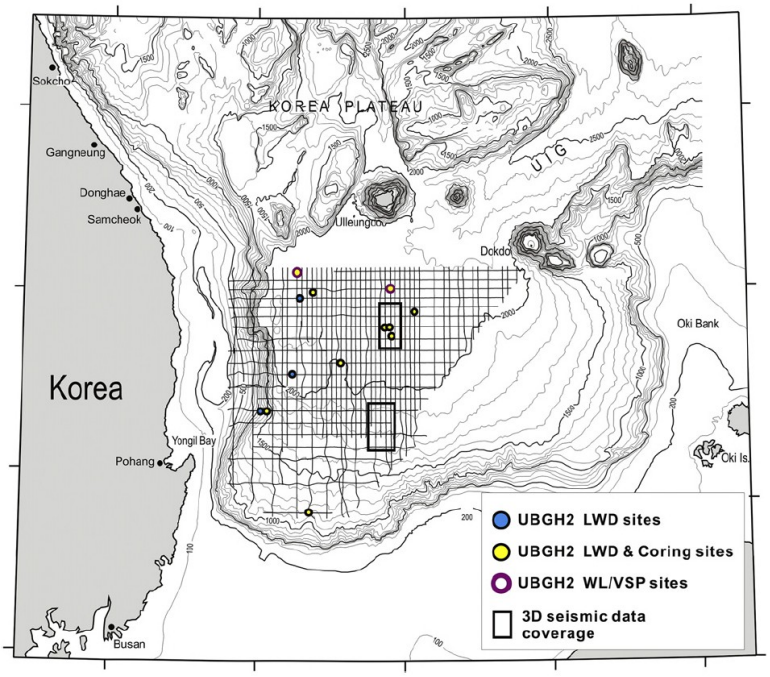

Figure 1. Bathymetry, 2-D seismic track lines, 3-D survey area (blocked) and drilling sites during the UBGH1 and UBGH2 scientific expeditions (from Matsumoto et al. 2011).

Surveys and analysis have indicated the layered sedimentary structure illustrated in Figure 2. The 12.7 m-thick hydrate reservoir is located 140m below the seafloor, spanning an area of 12 km^2. Above and below the hydrate bearing layers are very low permeability mud layers. The reservoir itself features layers of hydrate-free clays and hydrate-rich sands. The gas hydrate stability zone (BGHSZ) is 22.3m below the reservoir.

The reservoir can be described as a hybrid of a Class 2 reservoir and Class 3 reservoir (Moridis et al., 2007a; 2007b; 2011a; 2013). The Class 2 behavior is owed to the section with an overlying mobile water zone,

and the Class 3 behavior to the layers confined between low-permeability zones. The UBGH2-6 site is expected to manifest mostly Class 3 characteristics, as limited water mobility in the mud layers has been predicted (Moridis et al., 2013).

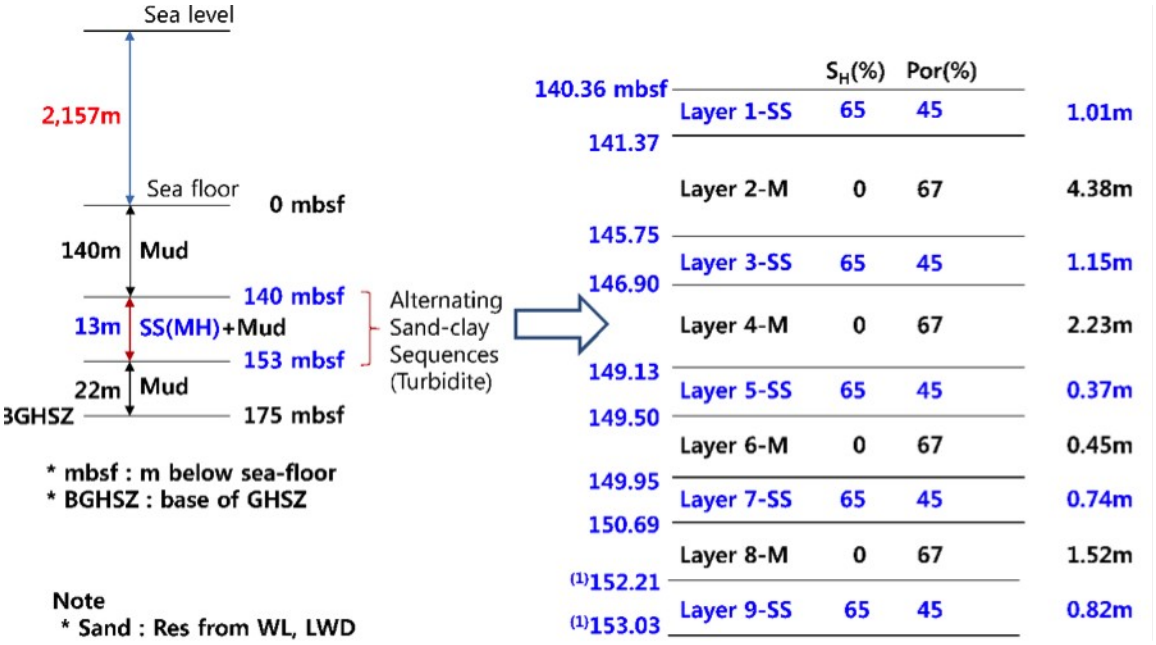

Figure 2. Geology, stratification, texture, dimensions and initial conditions in the subsurface at the UBGH2-6 site. The –M suffix in the layer description indicates mud; the –SS suffix indicates sand (Moridis et al., 2013).

2.2. Well design and production methodology

Depressurization is expected to be the most promising strategy for this site as with other Class 3 reservoirs (Moridis and Reagan, 2007a). Thermal stimulation has been explored in Moridis and Reagan (2007a) and shown to be an ineffective production strategy. The presence of low permeability layers in the region precludes the use of horizontal wells through the layer. Thus, in this study as in Moridis et al. (2013),

we use a simple vertical well with a perforated interval spanning the entire extent of the hydrate-bearing layers (Figure 3).

3. The Numerical Model and Simulation Approach

3.1. The numerical simulation codes

The TOUGH+Millstone suite was used to perform the coupled thermal, flow, and geomechanical analysis (Moridis et al., 2017). The first component of the suite is the extensively used TOUGH+HYDRATE simulator (Moridis et al., 2017), which has been used for numerous investigations of gas production from hydrates (Moridis et al., 2007; Moridis and Reagan, 2007b; Moridis and Reagan, 2011a; 2011b; Moridis and Reagan, 2007a; Moridis et al., 2011a; 2011b; Moridis and Sloan, 2007; Li et al., 2010). Due to the size and computational requirements of this system, the MPI-parallel pT+H simulator (Zhang et al., 2008) was used for the reservoir-scale simulations.

Millstone is a newly developed finite-element geomechanical simulator (Moridis et al., 2017) that offers the unique capability of both 3D and 2D axisymmetric formulations. It provides the functionality of automatically interpolating between different flow and geomechanical meshes to allow the use of unstructured grids without any adverse numerical problems. The TOUGH+Millstone suite can either be run fully coupled, in which the geomechanical response is calculated every

Newton iteration of the flow time stepping, or in a one-way coupled scheme, in which the geomechanical response is post-processed from snapshots of the flow simulation.

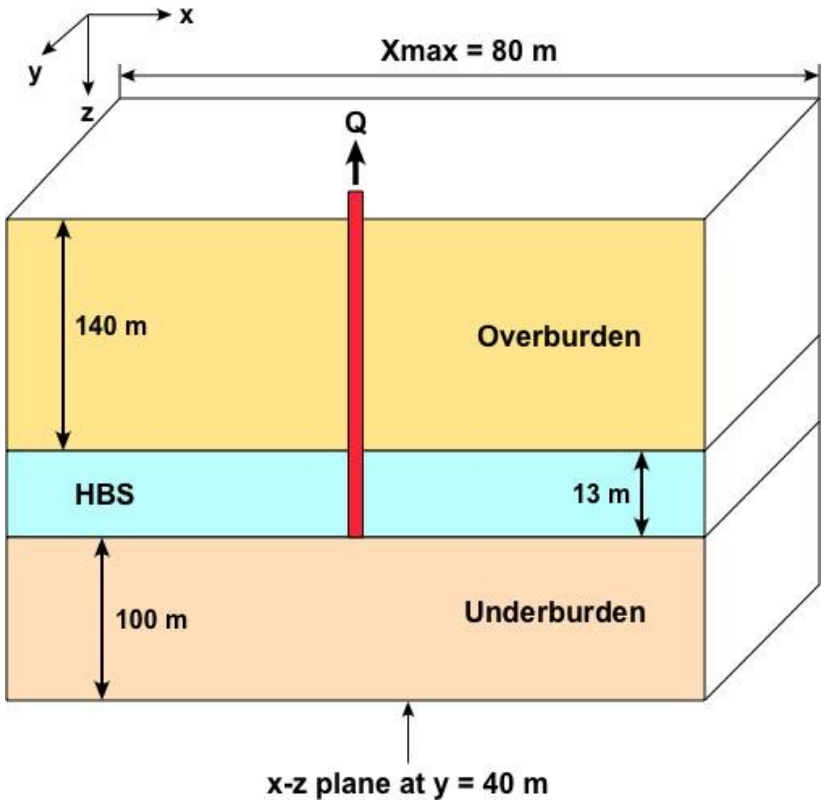

Figure 3. Description and dimensions of the 3D Cartesian domain used in the simulations. (Only the half-domain is shown, although the mesh includes the full domain. Not to scale)

3.2. Domain discretization

Very fine discretization was used near the wellbore and throughout the hydrate-bearing zones to capture the evolution of gas, water, and hydrate phases during production (Moridis et al., 2007). The two meshes used by TOUGH+ and Millstone are shown in Figure 4. The geomechanical domain is chosen to extend 300 m beyond the flow

mesh in x and y to minimize boundary effects, but has the same height in z. The 3D Cartesian domain of the single vertical well problem (see Figure 3) was discretized into 70 x 72 x 107 = 539,280 gridblocks in (x, y, z). Using equilibrium hydrate dissociation (Kowalsky and Moridis, 2007) and accounting for salinity, resulted in a system of about 2.16 x 10^6 equations. The geomechanical problem required linear systems with 50,313 equations for displacements and an additional 575,316 stress unknowns. Due to this size, the flow problem was simulated using MPI-parallel version of pT+H, and the geomechanical response was evaluated using a one-way coupling, where Millstone parsed the output flow fields from pT+H and solved the quasistatic evolution as a post-processing phase.

Discretization along the x- and y-directions was non-uniform, increasing logarithmically from the center of the system ($x = y = 40$ m) using a starting value of $\Delta x_0 = \Delta y_0 = 0.05$ m. Discretization along the z-axis was almost uniform (with $\Delta z = 0.1$-0.15m within the HBL) within the 12.67m of sand and clay/mud interlayers (Figure 2), as well as in the overburden and the underburden adjacent to the HBL. The discretization was non-uniform (with Δz increasing) in the overburden and underburden away from the HBL, with larger Δz near the top and bottom of the domain.

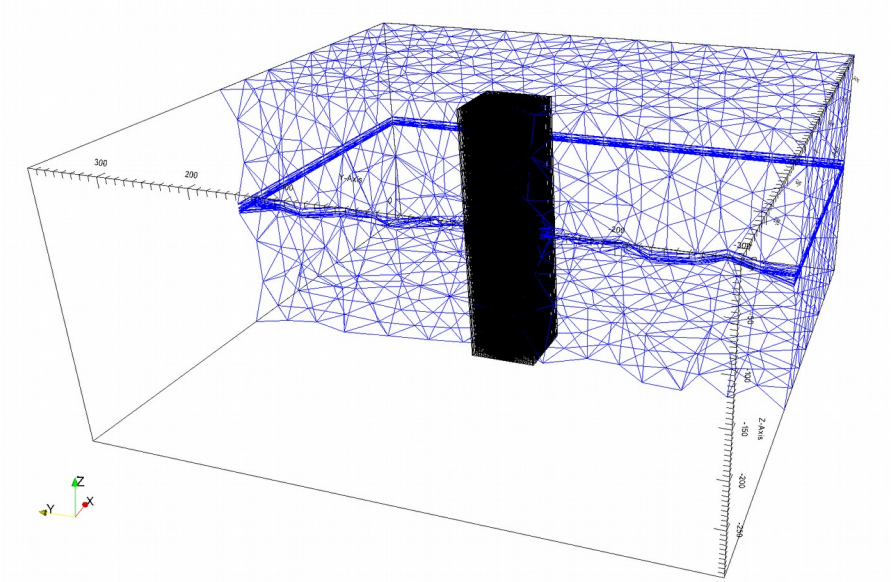

Figure 4. Domain of the flow problem as a TOUGH+ mesh domain (black, centered) inset in a larger geomechanical domain with a finite element mesh solved by Millstone (blue, cut halfway with extent outlined). Both meshes are unstructured, with more fine spacing near the center of the domain that is below the resolution of the image. Axes are in meters.

3.3. Baseline system properties and well description

The baseline hydraulic and thermal of the various geological media in the various layers of the geologic model in Figure 2, derived from laboratory studies and the literature, and the corresponding geomechanical properties are listed in Table 1. For the reference case, isotropic permeability conditions were assumed. The relative permeability and capillary pressure relationships and corresponding parameters were approximated based on similarly textured media. Note that the thermal conductivity values measured from samples from the UBGH2-6 site were very low, possibly due to the “watery” texture of the samples and their abnormally high porosity. We used

reasonable specific heat values for the various geologic media as direct measurements were unavailable.

The set of simulations included (a) a reference case based on the assumption of homogeneity and using the property values of Table 1, and (b) multiple realizations that involved statistical heterogeneity in the following key parameters:

- The intrinsic permeability k of the hydrate-bearing layers
- The porosity ϕ
- The hydrate saturation S_H

An extensive literature study indicated that heterogeneity in the (a) thermal and (b) geomechanical properties of geological media is far less pronounced than that of hydraulic properties, and that the thermal and geomechanical properties of formations vary within a remarkably narrow range. In the all the models of the heterogeneous distributions of the parameters discussed above, the mean values were those listed in Table 1. The statistical heterogeneity models and the standard deviations σ were as follows:

- The intrinsic permeability k of the HBL: *lognormal distribution*, $\sigma = 1$
- The porosity ϕ: *normal distribution*, $\sigma = 0.1$
- The hydrate saturation S_H: *normal distribution*, $\sigma = 0.1$

We approximated flow through the wellbore by Darcian flow through a pseudo-porous medium, as validated in previous studies (Moridis and Reagan, 2007b,c). This pseudo-medium has a porosity $\phi = 1$, a very high permeability $k = 5\text{x}10^{-9}$ m^2 (= 5,000 Darcies), a capillary pressure $P_c = 0$, relative permeability as a linear function of the phase saturations in the wellbore, and a low irreducible gas saturation $S_{irG} = 0.005$ (to allow the emergence of a free gas phase in the well).

3.4. Flow and thermal initial and boundary conditions

We determined the initial conditions in the reservoir by following the initialization process described by Moridis and Reagan (2007a,b). Direct measurements at the site indicate that te geothermal gradient is $dT/dz = 0.112$ °C/m. The uppermost and lowermost gridblock layers (i.e., at the ocean floor and at the bottom of the underburden) were treated as constant-pressure/constant-temperature open boundaries. The temperatures at the upper and lower boundaries, determined from field data, were $T_U = 0.482$ °C and $T_L = 51.180$ °C, respectively.

Using the known depth at the base of the hydrate system, and a hydrostatic pressure gradient, we calculated the pressure P_T using the P-, T-, and salinity-adjusted water density. Then, using P_T, the boundary temperatures, the hydrostatic gradient, and representative thermal conductivity values, we performed preliminary simulations to

determine the equilibrium *P*- and *T*-profiles and the initial state of the system.

Reservoir Porous Media Properties			
Overburden thickness		140 m	
Underburden thickness		147 m	
Layer thicknesses, porosities, S_H		As in Figure 2	
Initial pressure at top of domain (P_T)		22.261 MPa	
Initial temperature at top of domain (T_T)		0.482 °C	
Initial temperature at base of domain (T_B)		51.18 °C	
Gas composition		100% CH_4	
S_H in the hydrate-bearing sands		As in Figure 2	
Intrinsic permeability of sand k_r		1.78×10^{-13} m^2 (= 0.18 D)	
Intrinsic permeability of clay/mud overburden k_r		2e-18 m^2	
Intrinsic permeability of clay/mud underburden k_r		2e-19 m^2	
Intrinsic permeability of clay interlayers k_r		2e-16 m^2	
Grain density ρ_R (all formations)		2620 – 2660 kg/m^3 (mud); 2650 kg/m^3 (sand)	
Wet thermal conductivity ($k_{\Theta RW}$) (all formations)		1.45 W/m/K (sand), 1 W/m/K (muds)	
Composite thermal conductivity model (Moridis et al., 2008c)		$k_{\Theta C} = k_{\Theta RD} + (S_A^{1/2} + S_H^{1/2})(k_{\Theta RW} - k_{\Theta RD}) + \varphi S_I k_{\Theta I}$	
Capillary pressure model (vanGenuchten, 1980)		$P_{cap} = -P_0 \left[\left(S^* \right)^{-1/\lambda} - 1 \right]^{-\lambda}$ $S^* = \frac{\left(S_A - S_{irA} \right)}{\left(S_{mxA} - S_{irA} \right)}$	
S_{irA}		1	
λ		0.45 (sand); 0.15 (clay/mud)	
P_0		10^4 Pa (sand); 10^5 Pa (clay/mud)	
Relative permeability model - EPM (Moridis et al., 2008a)		$k_{rA} = (S_A^*)^n$ $k_{rG} = (S_G^*)^m$ $S_A^* = (S_A - S_{irA})/(1 - S_{irA})$ $S_G^* = (S_G - S_{irG})/(1 - S_{irA})$	
n; m		3.5; 2.5 (sand) 5.0; 3.0 (clay/mud)	
S_{irG}		0.01 (sand); 0.05 (clay/mud)	
S_{irA}		0.25 (sand); 0.55 (clay/mud)	
Constant bottomhole pressure BHP (P_w)		9 MPa	
BHP rate of decline to final level (dP_w/dt)		1 MPa/hr	
Reservoir Material Geomechanical Properties			
Layers	**Young's modulus**	**Bulk density**	**Poisson ratio**
Overburden (Mud A)	E=14 MPa	2620 kg/m^3	0.35
Hydrate zone	E=40 MPa (at S_H=0) E=1.4GPa (at S_H=1)	2650 kg/m^3	0.25
Underburden (Mud B)	E=20 MPa	2660 kg/m^3	0.35
Interlayer mud zones	E=18 MPa	2640 kg/m^3	0.35

Table 1. Physical properties used in the study of the UBGH2-6 deposit.

The numerical representation of a constant well P_w involves an internal boundary (an inactive element) at the uppermost element of the well. Here we impose a constant P_w, a thermal conductivity k_Θ = 0 W/m/K, and a constant temperature T_w, resulting in a constant bottomhole P_w In our study, the system behavior and performance was evaluated at a single value of P_w (= 9 MPa). Based on the results of earlier UBGH studies, this bottomhole pressure was the most desirable and practically attainable under the conditions of the UBGH2-6 deposit.

Constant-condition boundaries were placed on the *y*-*z* vertical planes at x = 0 and x = 80 m, and the *x*-*z* vertical planes at y = 0 and y = 80 m. The well radius in all studies was r_w = 0.1 m, and the well was centered about the $x = y$ = 40 m axis.

3.5. Geomechanical initial and boundary conditions

Roller boundary conditions are set at the x and y sides and the bottom side. The overburden pressure of 23.13 MPa is applied as the traction on the top boundary. The flow fields (P and S_H) at the beginning of production are used as the inputs to solve the initial static stress field of the mechanical system.

3.6. Simulation process

Following the methodology of previous studies in Moridis et al. (2013), the feasibility of the field test were evaluated by taking into account: 1) an absolute production criterion i.e. a potential for significant gas production; 2) a relative production criterion, seeking a low water/gas ratio; and 3) a geomechanical criterion, seeking a minimal degree of subsidence and preservation of the structural integrity of the well. Each simulated case was run for 14 days, the proposed length of the field test.

3.7. Simulation cases

A total of 8 different cases of various types and combinations of heterogeneity were investigated. These were the following:

(1) The reference (homogeneous) case with the properties of Table 1

(2) Three cases that each involved heterogeneity in a single parameter: k, φ and S_H, referred to as Cases k, ϕ, and S, respectively

(3) Three cases involving simultaneous heterogeneity in two parameters, i.e., k and ϕ, k and S_H, and φ and S_H, referred to as Cases $k\phi$, kS, and ϕS, respectively

(4) A case involving heterogeneity in all three parameters, i.e., k, ϕ and S_H, referred to as Case $k\phi S$

We considered two material groups: a sandy (hydrate-bearing) medium, and a clay (mud) medium of the overburden, underburden

and of the interlayers between the sandy hydrate-bearing sediments (HBS). The relevant geomechanical properties are listed in Table 1. For Young's modulus we used linear functions of S_H in the hydrate-bearing media. We used a constant Poisson's ratio and the Biot coefficient was $b = 0.8$. (Rutqvist and Moridis, 2009; Rutqvist et al., 2009).

4. Production Behavior

4.1. Gas releases from dissociation

Figure 5 shows the expected evolution of the release rate Q_R during the planned 14-day test as a result of the depressurization caused by the operation of a single vertical well at the center of the Cartesian domain. Figure 5 reveals that (a) the rates Q_R of all cases in the figures increase monotonically during the duration of the test, but (b) the release rates are rather low during the production period. In terms of overall performance, the 8 cases we investigated can be classified in three general groups, with roughly the same Q_R for all cases in each group. The high-Q_R group includes only Case ϕ; the average-Q_R group includes 3 cases (Cases k and $k\phi$, as well the reference case); and the low-Q_R group is the largest, including 4 cases (Cases S, kS, ϕS and $k\phi S$).

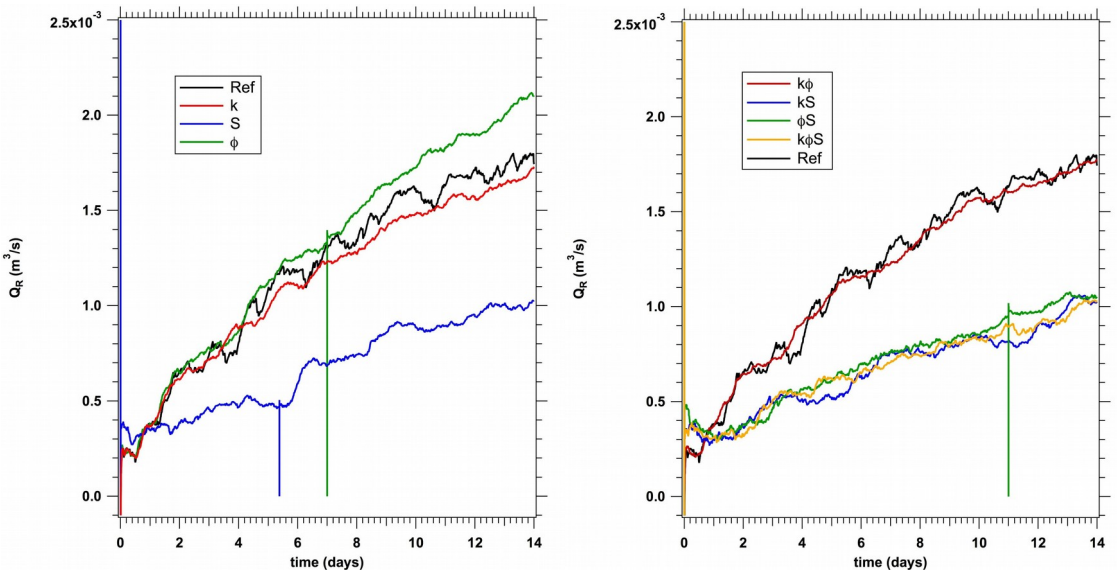

Figure 5. Expected evolution of the rate of gas release from dissociation (Q_R) over time during the planned 14-day test for reference, k, S and ϕ.cases (left), and reference, kϕ, kS, ϕS and kϕS (right).

The conclusions that can be drawn regarding the effects of statistical heterogeneity are the following:

- Heterogeneity in the porosity ϕ is the only state that results in a mild increase in Q_R over than in the reference case.
- Heterogeneity (a) in k and (b) simultaneously in both k and ϕ appear to have minimal to practically no effect on Q_R compared to the reference case.
- Heterogeneity (a) in S, (b) simultaneously in both k and S, (c) simultaneously in both ϕ and S and (b) simultaneously in all three variables (k, ϕ and S) have a significant negative effect on Q_R compared to the reference case. Thus, ϕ, heterogeneity in which

by itself increases Q_R, does not enhance Q_R when combined in heterogeneity with the other variables.

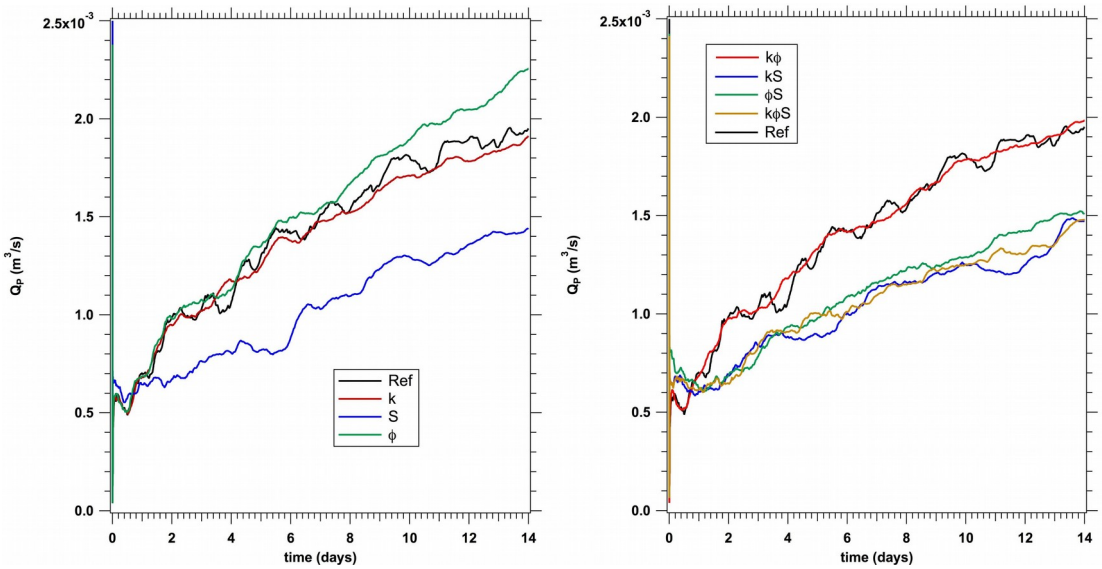

Figure 6. Expected evolution of the rate of gas production (Q_P) over time during the planned 14-day test in the following cases: reference, k, S, and ϕ.(left), and kϕ, kS, ϕS and kϕS(right). Note the modest production rates.

4.2. Gas production

Figure 6 shows the expected evolution of the production rate Q_P for all cases during the planned 14-day test. Note that the Q_P depicted in these figures represents the total gas production rate, including both CH_4 in the gas phase and dissolved in the aqueous phase.

The production rates Q_P appear quite similar in pattern and magnitude to those in Figure 5 leading to similar observations and conclusions. We see that (a) the rates Q_P of all cases increase monotonically during the duration of the test, but (b) the rates are low during the early

production period. Compared to the Q_R curves, the corresponding Q_P curves are generally higher, indicating significant contributions of dissolved gas to total gas production. The three general groups into which we classified the Q_R behavior persist in Q_P: the higher-performance group that includes only Case ϕ; the average-performance group that includes 3 cases (Cases k and $k\phi$, as well the reference case); and the lower-performance group, which is the largest and includes 4 cases (Cases S, kS, ϕS and $k\phi S$).

The similarity of the Q_R and Q_P behavior leads to similar conclusions regarding the effects of statistical heterogeneity (as described by the statistical models, the means and standard deviations of the considered variables):

- Heterogeneity in the porosity φ is the only one that results in a mild increase in Q_R over than in the reference case.
- Heterogeneity (a) in k and (b) simultaneously in both k and ϕ appear to have minimal to practically no effect on Q_P compared to the reference case.
- Heterogeneity (a) in S, (b) simultaneously in both k and S, (c) simultaneously in both ϕ and S and (b) simultaneously in all three variables (k, ϕ and S) have a significant negative effect on Q_P compared to the reference case. Thus, ϕ, heterogeneity in which

by itself increases Q_P, does not enhance Q_P when combined in heterogeneity with the other variables.

The cumulative volumes V_R of produced CH_4 for all cases during the planned production 14-day test in Figure 7 confirm conclusively the groupings identified in the analysis of the Q_R and Q_P from Figures 4 and 5, and show low produced CH_4 volumes for all cases.

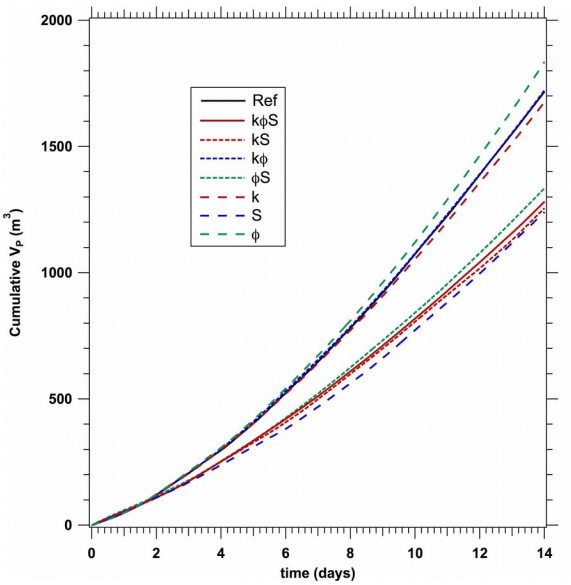

Figure 7. Evolution of cumulative volume of produced gas (V_P) over time during the planned 14-day test (all cases). Note the modest cumulative volumes.

4.3. Water production

Figure 8 shows the evolution of the water production rate Q_w at the well for all cases, and confirms the earlier groupings into which the

effects of heterogeneity have been classified (Sections 4.1 and 4.2). The higher- and lower-performance groups are shown to be associated with the higher Q_w, and the mid-level Q_w is associated with average-performance group.

4.4. Water-to-Gas ratio

Figure 9 presents the instantaneous and cumulative water-to-gas ratios for the 14-day production period. The instantaneous water-to-gas ratios, R_{WGi}, (Figure 9 left) appear to stabilize early (after 2-3 days) to an average value of about 85. This indicates a negative production regime during the 14-day test because of the disproportionate large amount of produced water compared to the produced gas. It is possible that the short duration of the planned test may not allow sufficient time for significant gas release and production and a longer test is necessary before conclusive evidence of the behavior of R_{WGi} becomes apparent. For reference, promising (for production) hydrate deposits exhibit an initial R_{WGi} of about 20, which is reduced asymptotically toward ~4 during long-term production.

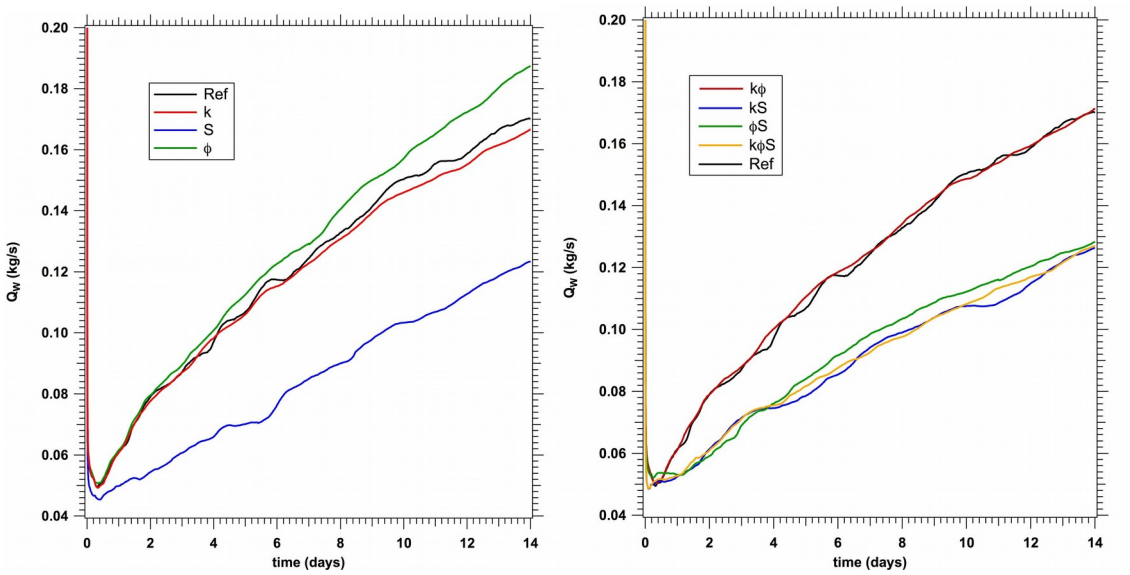

Figure 8. Expected evolution of the rate of water production (Q_W) over time during the planned 14-day test in the following cases: reference, k, S and ϕ (left), and reference, kϕ, kS, ϕS and kϕS (right).

In Figure 9 (right), the cumulative water-to-gas ratios R_{WGc} (= M_W/V_P) exhibit different behavior. While cases in the lower-performance group show a distinctive pattern marked by a initial sharp drop (indicating higher initial gas releases, usually associated with a sharper initial pressure drop), followed by a slow rise and eventual stabilization after about 6 days, the higher- and average-groups have similar behavior that is characterized by an initial sharp decline followed by stabilization (at about the same level as the lower-performance group). As in the R_{WGi} case, the stable R_{WGc} level is about 85, which is very high and does not indicate a favorable production regime during the 14-day test.

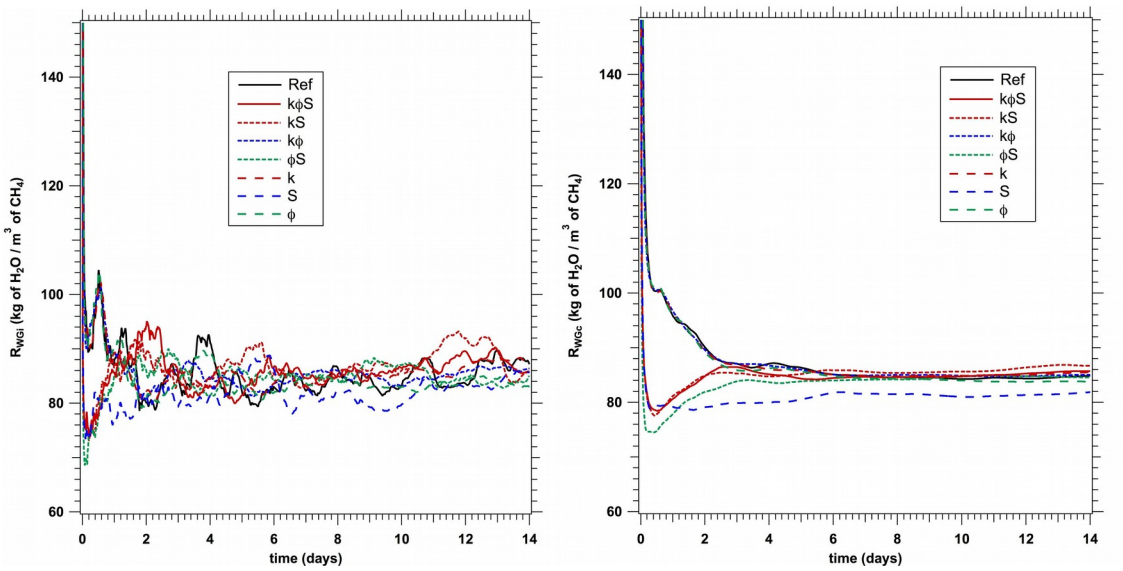

Figure 9. Evolution of the instantaneous (left) and cumulative (right) Water-to-Gas Ratios ($R_{WGi} = Q_W/Q_P$) over time during the planned 14-day test (all cases).

5. Spatial distributions

All the spatial distributions that we discuss in this Section are associated with Case $k\phi S$, in which all three variables are simultaneously heterogeneous according to the specifics discussed in Section 3.3.

5.1. *P*-distribution

The pressure distributions at t = 1, 5, 10 and 14 days in Figure 10 provide a clear depiction of the heterogeneous nature of the hydrate reservoir and confirms that the size of the domain was sufficient to capture the system behavior during the 14-day production test. As expected, the largest pressure drops occur close to the vertical well. Horizontal discontinuities in the *P*-distribution indicate the locations of

the low-*k* mud layers. Localized patches of higher pressure are due to heterogeneous regions of higher S_H (exhibiting very low effective permeability). Because of the limited duration of the test, the pressure disturbance does not advance deep into the body of the hydrate. Actually, the pressure appears relatively undisturbed (from its original level) at $x > 15$ m. This has significant implications for the location of observation wells.

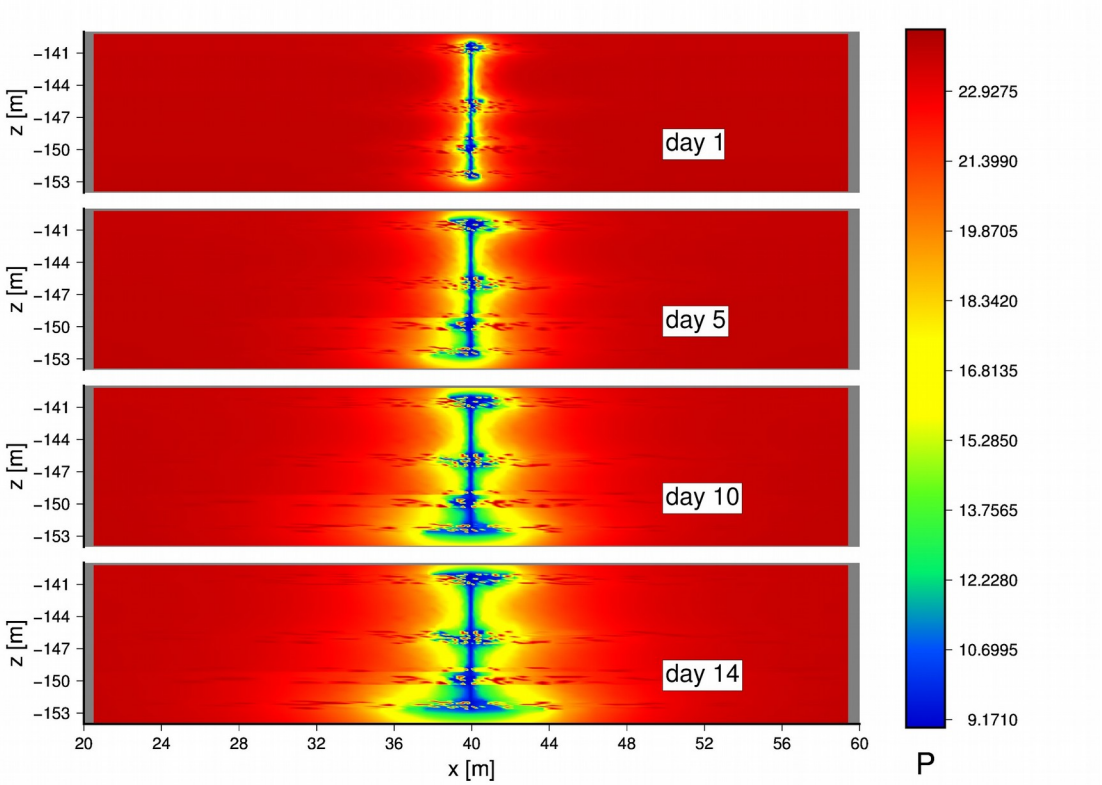

Figure 10. Case kϕS: Pressure (in MPa) distributions on the *x*-*z* plane at y = 40 m during the 14-day long production test (P_w = 9 MPa).

5.2. *T*-distribution

The temperature distributions in Figure 11 provide an indication as to the location of the maximum dissociation activity, where maximum cooling occurs as a result of the endothermic nature of hydrate

dissociation. The temperature distributions in Figure 11 also provide some insight as to the location of a possible observation well because no temperature disturbance (from its original level) is observed at $x >$ 15 m. This also highlights the limited extent of hydrate dissociation during the 14-day test.

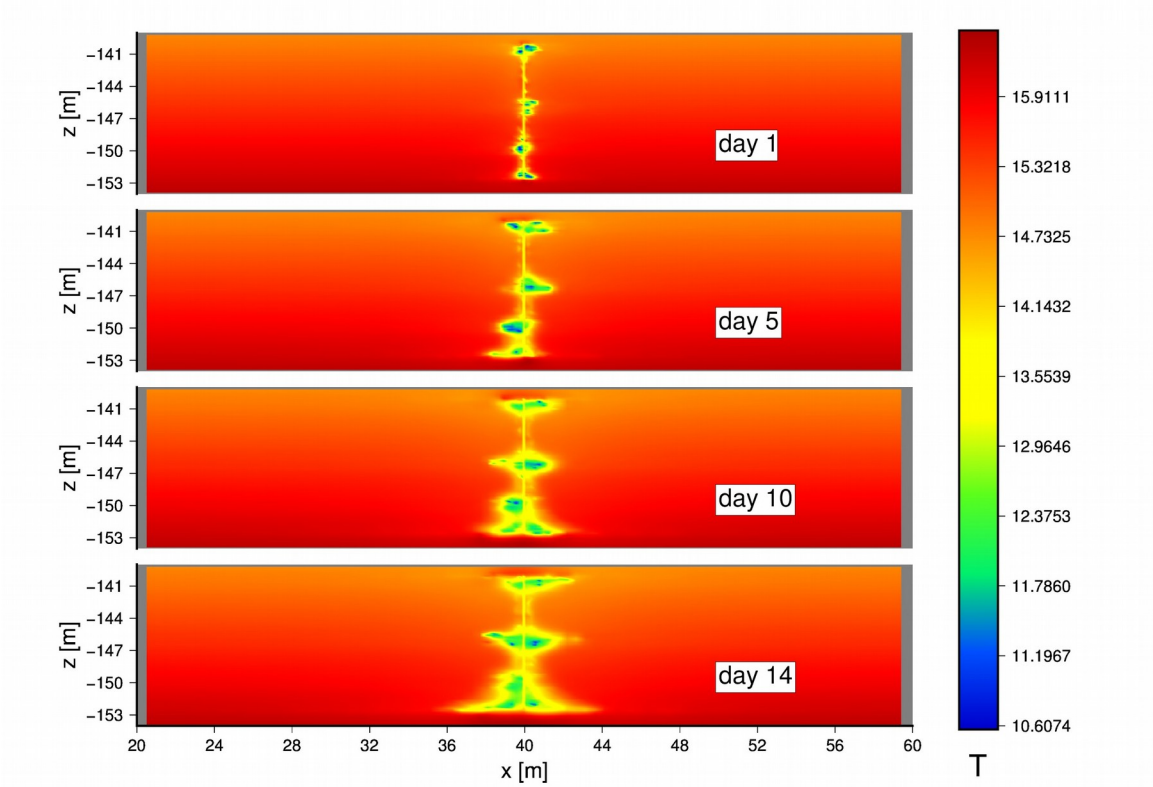

Figure 11. Case kϕS: Temperature (in ºC) distributions on the x-z plane at y = 40 m during the 14-day long production test (P_w = 9 MPa).

5.3. S_H and S_G distributions

The evolution of the S_H (Figure 12) and S_G (Figures 13) distributions show the limited dissociation of the sandy HBS, and the corresponding evolution and distribution of gas. Hydrate dissociation extends only

about 5 m from the well, with the exception of thin layers adjacent to the mud interlayers (which provide a source of heat to create upper and lower hydrate dissociation interfaces). Local heterogeneity in S_H results in isolated patches of hydrate that remain for some time after the main dissociation front passes, and the effect of the three-parameter heterogeneity is apparent in the irregular patterns of dissociation. The evolution of free gas is limited, S_G is relatively low after 14 days, and the gas is confined to a region within a short distance around the well.

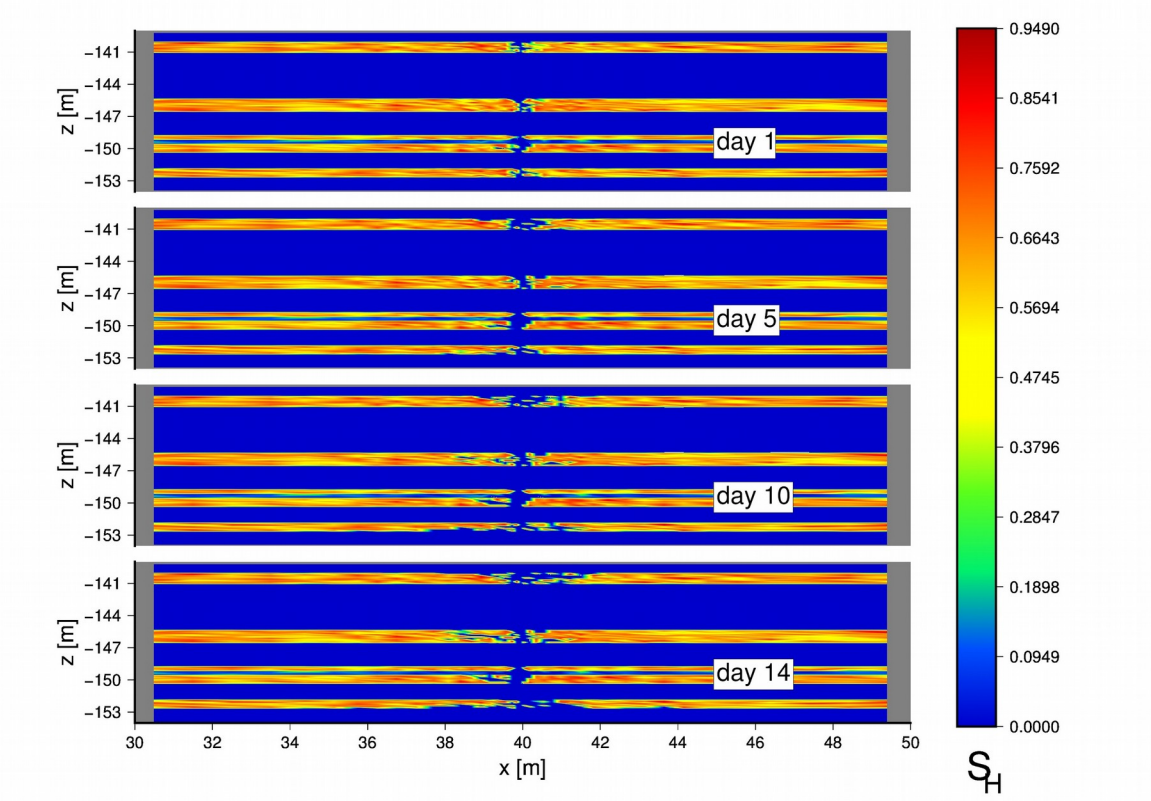

Figure 12. Case kϕS: Hydrate saturation (S_H) distributions on the x-z plane at y = 40 m during the 14-day long production test (P_w = 9 MPa).

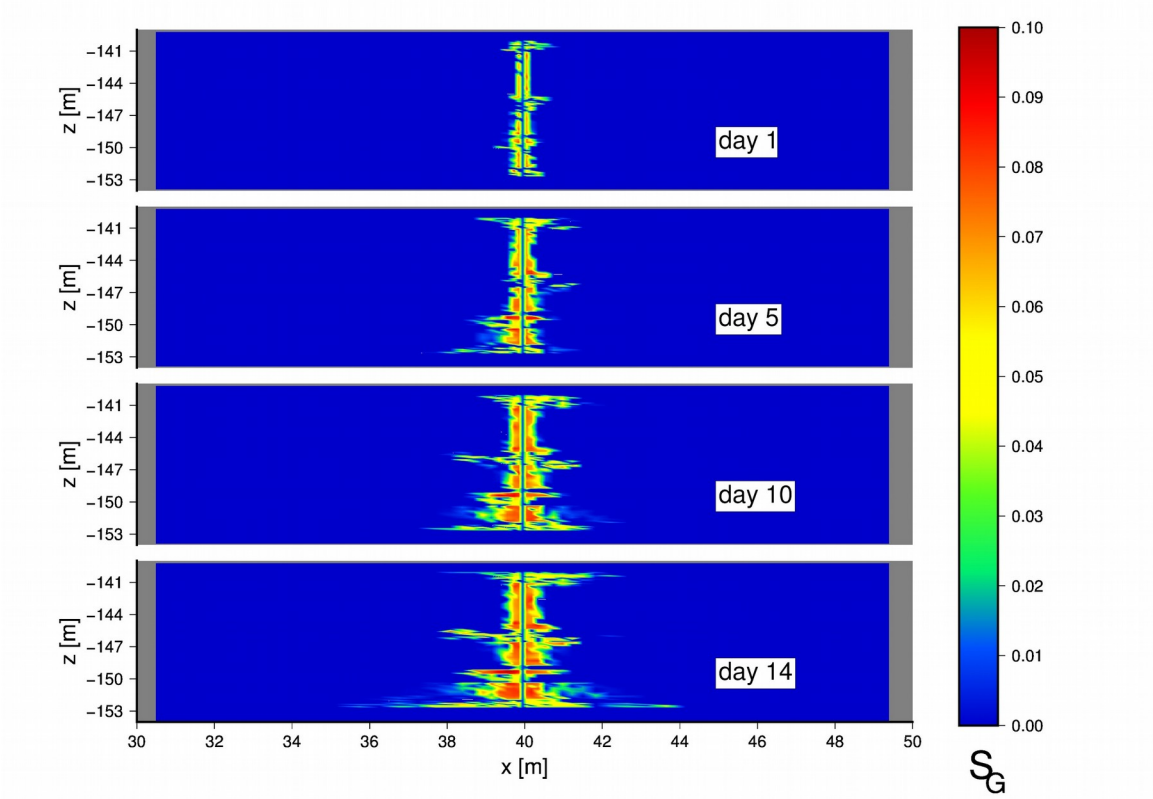

Figure 13. Case kϕS: Gas saturation (S_G) distributions on the x-z plane at y = 40 m during the 14-day long production test (P_w = 9 MPa).

6. Geomechanical system behavior

To evaluate the geomechanical stability of the reservoir, the possibilities of subsidence or uplift are analyzed. The displacements are probed at the seafloor (z = 0 m), top of the HBS (z = -140 m), and base of the HBS (z = -153 m). The time response of the vertical displacements are plotted in Figure 14 for both the homogeneous reference case and heterogeneous $k\phi S$ case, yielding similar results at each of the locations. The subsidence at the seafloor is minimal in both cases, less than 2 cm, though the reference case is noticeably larger.

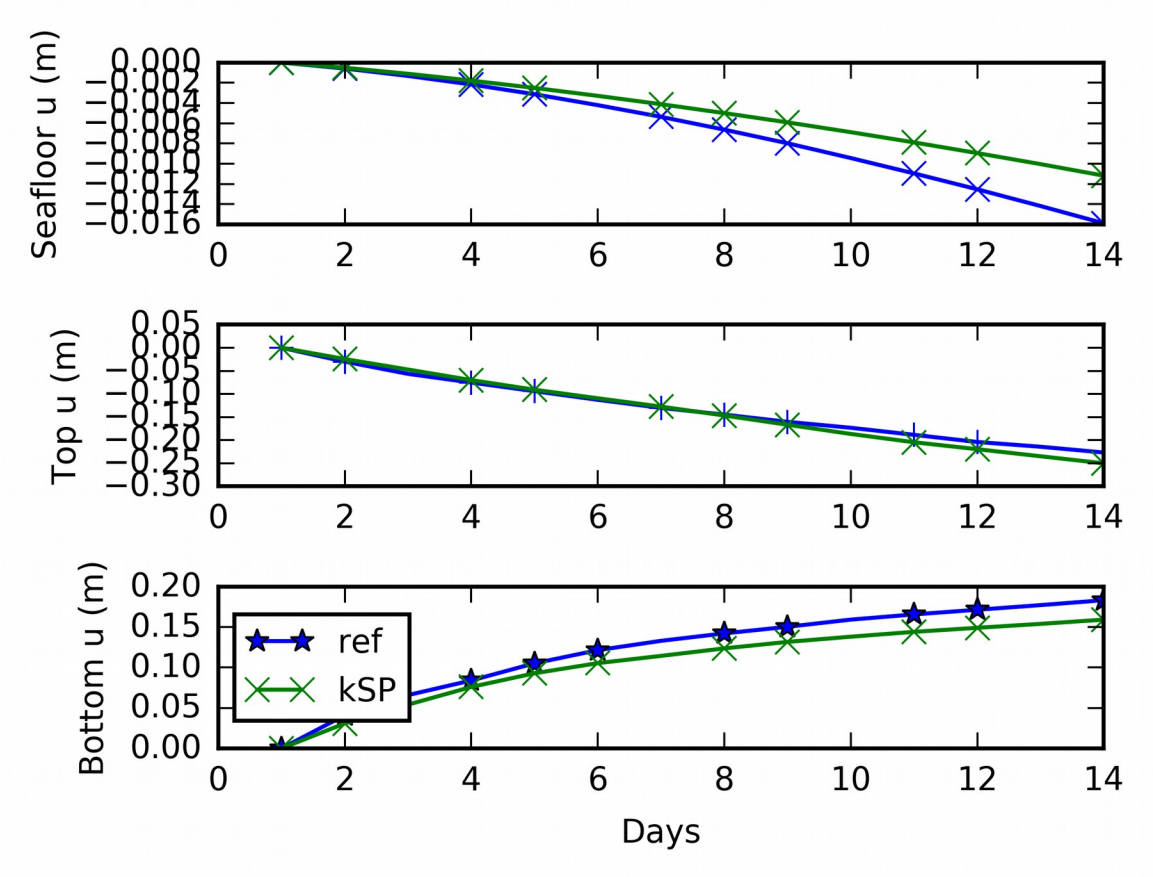

Figure 14: Vertical displacement history of the system of both cases at the seafloor (z = 0 m), top of the reservoir (z = -140 m), and bottom of the reservoir (z = -153 m).

The displacement field at the end of production for the heterogeneous $k\phi S$ case is rendered on a cross section through the vertical well along the *y*-*z* plane and shown in Figure 15. The maximum displacements are observed to be at the top and bottom of the HBS along the axis of the well. The base of the HBS registers a significant uplift in both cases with a value of and 0.159 m and 0.183 m in the $k\phi S$ case and reference case, respectively. The maximum displacement is observed at the top of the reservoir, with a maximum value of 0.226 m in the uniform

reference case. It is additionally observed in Figure 15 that the reservoir contracts significantly into the well, with the maximum inward motion occurring in the bottom most interlayer.

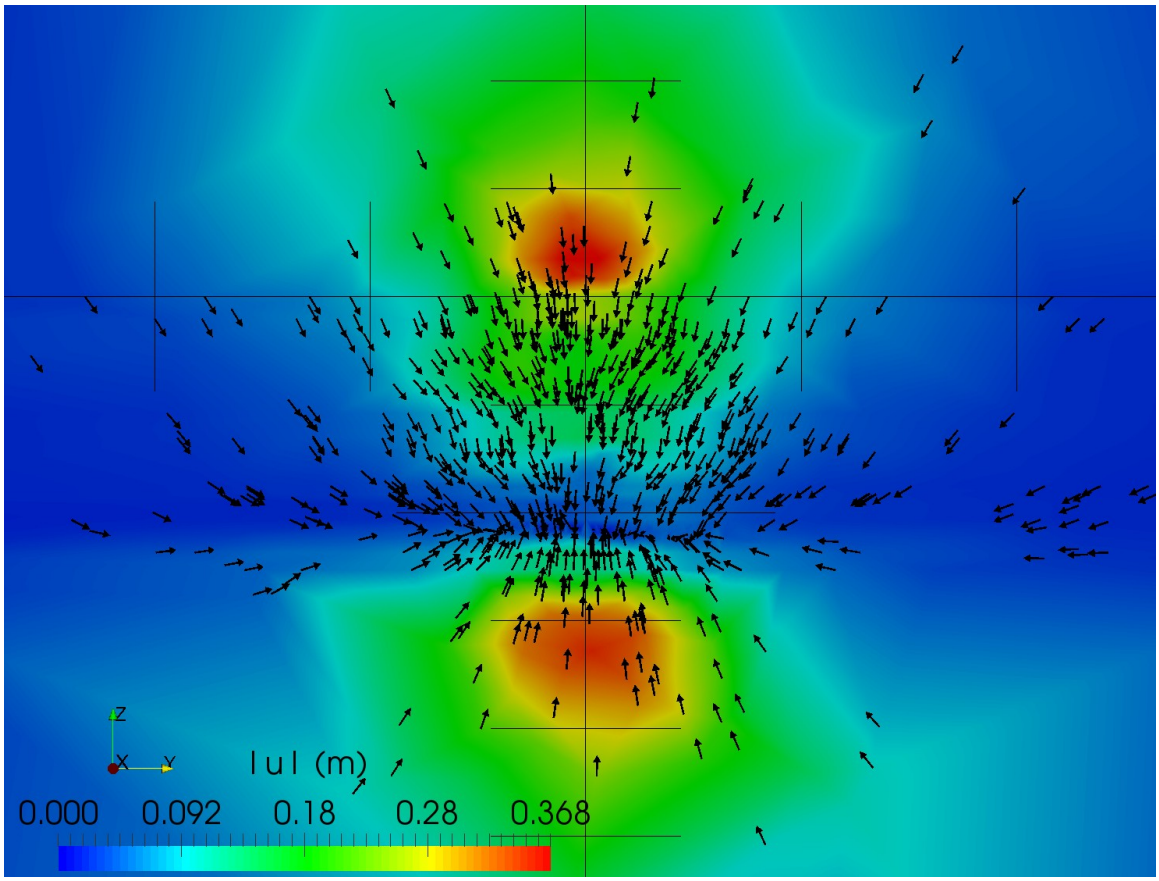

Figure 15. Displacement field at the well center at the end of production for the heterogenous $k\phi S$ case. The mesh is colored by the magnitude of the displacement through the cross section, and the arrows indicate direction of the displacement. The horizontal axis grid passes through the top of the producing layers (z = -143 m) and the tic marks are every 5 m.

7. Conclusions and Discussion

We draw the following conclusions from this study:

- Gas production from a hydrate accumulation with the characteristics of the UBGH2-6 site is *technically* feasible.
- The analysis of the impact of statistical heterogeneity was focused on three parameters: HBS intrinsic permeability k, porosity φ and initial hydrate saturation S_H. The effects of heterogeneity, in terms of overall performance, can be classified in three general groups: the **higher-performance** group that includes only Case φ; the **average-performance** group that includes 3 cases (Cases k and $k\varphi$, as well the reference case); and the **lower-performance** group, which includes 4 cases (Cases S, kS, φS and $k\varphi S$). The behavior of each member of these groups is otherwise similar.
- The gas release and production rates are generally low and the affected region of the reservoir is limited. Water production appears manageable (in terms of absolute rates and volumes) under all of the scenarios investigated in this study; however, in relative terms the water-to-gas ratio is very high during the 14-day production test and stabilizes relatively early.
- The maximum subsidence at the seafloor is predicted to be 0.016m, but the maximum subsidence and uplift of the top and bottom of the reservoir, respectively, is predicted to have a magnitude of 0.22m.

- Assumption of heterogeneity decreases the magnitude of the geomechanical response.

Areas for future research may include:

- Analysis of system performance and gas production predictions when more detailed information becomes available on the subsurface stratigraphy and porous media properties (flow and geomechanical) based on direct measurements and observations.
- Evaluation of alternative sites within the Ulleung basin or in the wider Korean Exclusive Economic Zone.

Acknowledgments and Data

This work was supported by the Korea Institute of Geoscience and Mineral Resources, and by the Assistant Secretary for Fossil Energy, Office of Natural Gas and Petroleum Technology, through the National Energy Technology Laboratory, under the U.S. Department of Energy, Contract No. DE-AC02-05CH11231. The TOUGH+ and Millstone software used in this study may be acquired through the Berkeley Lab Software Center (https://blsc.lbl.gov/). Parameters used in the T+H/Millstone runs described in this paper are listed in Table 1 and the reference cited therein. Unprocessed simulation outputs are archived at https://github.com/mtreagan/TOUGH-HYDRATE-repo/.

References

Chough, S.K., Lee, H.J., and Yoon, S.H. 2000. *Marine Geology of Korean Seas*, 2nd edition, Chap. 3, Sec. 3.13. Amsterdam, The Netherlands: Elsevier Science B.V

Kim, J., G.J. Moridis, and J. Rutqvist, 2012a. Coupled Flow and Geomechanical Analysis for Gas Production in the Prudhoe Bay Unit L-106 Well Unit C Gas Hydrate Deposit in Alaska, *Journal of Petroleum Science and Engineering*, **92-93,** 143-157 (doi: 10.1016/j.petrol.2012.04.012

Kim J., Moridis G., Yang D., and Rutqvist J. 2012b. Numerical studies on two-way coupled fluid flow and geomechanics in hydrate deposits, *Soc. Pet. Eng. J.*, **17**(2): 485–501.

Kowalsky, M. B., and G.J. Moridis, 2007. Comparison of kinetic and equilibrium reactions in simulating the behavior of gas hydrates, *Energy Conversion and Management*, **48**, 1850, doi:10.1016/j.enconman.2007.01.017.

Li, G., G.J. Moridis, K. Zhang and X.-S. Li, Evaluation of Gas Production Potential from Marine Gas Hydrate Deposits in Shenhu Area of the South China Sea, *Energy & Fuels*, **24**, 6018-6033, 2010 (doi: 10.1021/ef100930m)

Makogon, Y.F., 1997. *Hydrates of Hydrocarbons*. Penn Well Publishing Co. Tulsa, OK.

Matsumoto, R., B.J. Ryu, S.R. Lee, S. Lin, S. Wu, K. Sain, I. Pecher, and M. Riedel, 2011. Occurrence and exploration of gas hydrate in the marginal seas and continental margin of the Asia and Oceania region, *Marine and Petroleum Geology* **28**, 1751-1767, doi: 10.1016/j.marpetgeo.2011.09.009.

Moridis, G.J. and E.D. Sloan, 2007. Gas Production Potential of Disperse Low-Saturation Hydrate Accumulations in Oceanic Sediments, *J. of Energy Conversion and Management***, 48(**6**,** 1834-1849, doi: 10.1016/j.enconman.2007.01.23.

Moridis, G.J., Kowalsky, M.B., Pruess, K., 2007. Depressurization-induced gas production from Class 1 hydrate deposits. *SPE Res. Eval. Eng*. **10** (5): 458-481.

Moridis, G.J., and Reagan, M.T., 2007a. Strategies for Gas Production From Oceanic Class 3 Hydrate Accumulations, *OTC-18865*, 2007 Offshore Technology Conference, Houston, Texas, 30 April – 3 May 2007.

Moridis, G.J., and Reagan, M.T., 2007b. Gas Production From Oceanic Class 2 Hydrate Accumulations, *OTC 18866*, 2007 Offshore Technology Conference, Houston, Texas, U.S.A., 30 April–3 May 2007.

Moridis, G.J., Kowalsky, M., and Pruess, K., 2007. Depressurization-Induced Gas Production From Class 1 Hydrate Deposits, *SPE Reservoir Evaluation and Engineering*, **10**(5), 458-488.

Moridis, G.J., Kowalsky, M.B., and Pruess, K., 2008. TOUGH+HYDRATE v1.0 User's Manual: A Code for the Simulation of System Behavior in Hydrate-Bearing Geologic Media, Report LBNL-00149E, Lawrence Berkeley National Laboratory, Berkeley, CA.

Moridis, G.J., M.T. Reagan, S.-J. Kim, Y. Seol and K. Zhang, 2009. Evaluation of the Gas Production Potential of Marine Hydrate Deposits in the Ulleung Basin of the Korean East Sea, *SPE Journal,* **14**(4): 759-781, doi: 10.2118/110859-PA.

Moridis, G.J., and M.T. Reagan, 2011a. Estimating the Upper Limit of Gas Production From Class 2 Hydrate Accumulations in the Permafrost, 1: Concepts, System Description and the Production Base Case, *J. Petr. Sci. Eng.*, 76, 194-201, (doi:10.1016/ j.petrol.2010.11.023).

Moridis, G.J., and M.T. Reagan, 2011b. Estimating the Upper Limit of Gas Production From Class 2 Hydrate Accumulations in the Permafrost, 2: Alternative Well Designs and Sensitivity Analysis, *J. Petr. Sci. Eng.*, 76, 124-137, 2011b (doi: 10.1016/j.petrol. 2010.12.001).

Moridis, G.J., Reagan, M.T., Boyle, K.L., and K. Zhang, 2011a, Evaluation of the Gas Production Potential of Some Particularly Challenging Types of Hydrate Deposits, *Transport in Porous Media*, 90 (1), 269-299, doi: 10.1007/s11242-011-9762-5.

Moridis, G.J., Silpngarmlert, S., Reagan, M.T., Collett, T., Zhang, K., 2011b. Gas production from a cold, stratigraphically bounded hydrate deposit at the Mount Elbert site, North Slope, Alaska. *J. Marine Petr. Geol*., 28, 517-534 (doi: 10.1016/j.marpetgeo.2010.01.005)

Moridis, G.J., M.T. Reagan, K.L. Boyle, and K. Zhang, 2011d. Evaluation of the Gas Production Potential of Challenging Hydrate Deposits, *Transport in Porous Media*, 90, 269-299 (doi: 10.1007/s11242-011-9762-5).

Moridis, G.J., Kim, J., Reagan, M.T., Kim, S.J. 2013. Feasibility of Gas Production from a Gas Hydrate Accumulation at the UBGH2-6 Site of the Ulleung Basin in the Korean East Sea, *J. Petro. Sci. Eng*., doi: 10.1016/j.cageo.2013.04.001, 2013.

Moridis, G. J., A. F. Queiruga, and M. T. Reagan, 2016. The T+H+M Code for the Analysis of Coupled Flow, Thermal, Chemical and Geomechanical Processes in Hydrate-Bearing Geologic Media, 9th International Gas Hydrates Conference, Denver, CO, June, 2016.

Rutqvist J. and G.J. Moridis, 2009. Numerical studies on the geomechanical stability of hydrate-bearing sediments, *Soc. Pet. Eng. J.*, **14**(2), 267–282 (doi: 10.2118/126129-PA).

Rutqvist J., Moridis G.J. and T. Grover, 2009. Geomechanical response of permafrost-associated hydrate deposits to depressurization-induced gas production, *J. Pet. Sci. Eng.,* **67**, 1-12.

Sloan, E.D. and C.A. Koh, 2008. *Clathrate hydrates of natural gases*, 3rd Edition: CRC Press, Taylor and Francis Group, Publishers, New York, New York.

Zhang, K., and Moridis, G.J., 2008. A Domain Decomposition Approach for Large-Scale Simulations of Coupled Processes in Hydrate-Bearing Geologic Media**,** paper presented at the 6th International Conference on Gas Hydrates, Vancouver, British Columbia, Canada, July 6-10, 2008.